Chapter 2
High pressure setup for optical phase difference measurements

2.1 Introduction

Phase transitions in liquid crystals are usually studied by varying temperature at atmospheric pressure. As the liquid crystalline materials are soft, even moderately high pressures often have a strong influence on the transition temperatures. As the average intermolecular distance *r* is decreased by the application of pressure the relative importance of volume and temperature on various phase transitions can be evaluated, and compared with the relevant theoretical models. Effect of compression on phase transitions in liquid crystals has been investigated for more than a century [1,2]. In1899, within a decade of the discovery of liquid crystals, Hulett [3] had conducted the first high pressure experiments (upto 300 bars) on three compounds viz., p-azoxyanisole (PAA), p-azoxyphenetole (PAP) and cholesteryl benzoate [3]. The pressure was generated by a pump and transmitted to the sample held inside a capillary tube by mercury and the phase transitions observed visually. In the next seventy years only two more pressure studies were reported, one by Puschin and Grebenschtschikow [4] in 1926 and the other by Robberecht in 1938 [5]. But since 1970s there has been a considerable growth in this field and a number of interesting phenomena such as pressure induced mesomorphism, suppression of mesophase, re-entrant phenomena have been discovered [1,2]. Optical transmission technique was the earliest method used to detect the phase transitions at high pressures [3,5]. This technique has been used with considerable success by Keyes et al [6], Cladis et al [7] and Kalkura et al [8]. All these studies have been conducted using cells which have been designed for forward scattering measurements. A phase transition between two mesophases is associated with a textural change. Some of the high pressure (HP) optical setups reported in the literature viz., those by Pollmann [9], Illian et al [10], Carboni et al [11,12] offer the advantage of observing the sample under high pressure through a polarising microscope. The HP optical setups reported in reference [9,11,12] can also be used for the measurement of selective reflection spectra. There have also been a few studies on the variation of orientational order parameter *S* with temperature at elevated pressures, using NMR [13-15], Raman spectroscopy [16] and

optical birefringence measurements [17]. More recently Urban and co-workers have taken up a systematic investigation on the influence of pressure on the dielectric anisotropies of several nematogens [18,19]. In the earlier high pressure (HP) studies conducted in our laboratory [8], phase transitions were detected by monitoring the intensity of a laser beam passing through the liquid crystal sample using a photo detector. As liquid crystalline phase transitions are associated with textural changes there would be an abrupt change in the intensity of the transmitted light at the phase transition point.

The design of the experimental setup for HP investigations of liquid crystals present certain special problems which are not usually encountered in the study of solids. Even a small contamination by the pressure transmitting medium of the liquid crystal sample results in a significant reduction of various transition temperatures. In our laboratory Kalkura et al [8] designed and fabricated a HP optical cell for studying phase transitions of liquid crystals. We present a brief description of the HP optical setup as adapted from reference [8]. We have modified the HP optical setup so that the optical path-difference of an aligned sample can be measured as functions of both temperature and pressure. In this chapter we report the estimated order parameters of some nematic and smectic A liquid crystals as functions of both pressure and temperature using this modified setup.

2.2 Experimental

2.21 Description of the HP cell

A schematic diagram of the basic parts of high pressure (HP) optical cell is given in Figure 2.1. All the components of the cell are machined using a low alloy hardenable Indian steel, viz., EN-24 (equivalent to AISI 4130) which has 0.4% carbon, 0.2% silicon and 0.55% nickel. This steel has the advantage that it can be hardened to great strengths by means of martensitic transformation. The alloying elements increase the hardenability of the material and in addition, also contribute to the strength by solid solution strengthening. The different parts of the cell are machined and heat treated to strength ranging from 40 to 55 RC depending on the component and its location in the cell. (Rockwell C scale (RC) is the most commonly used hardness scale. The RC scale is calculated from the depth of indentation caused

by a 120-degree-angle pyramid shaped diamond cone under a constant 150Kg load). The body of the cell has threaded openings on both sides into which two plugs with exactly matching threads can be fitted. On the outside, the plugs have a large tapered opening (70^0 outside taper) which facilitates a wide viewing angle without affecting the strength of the plug.

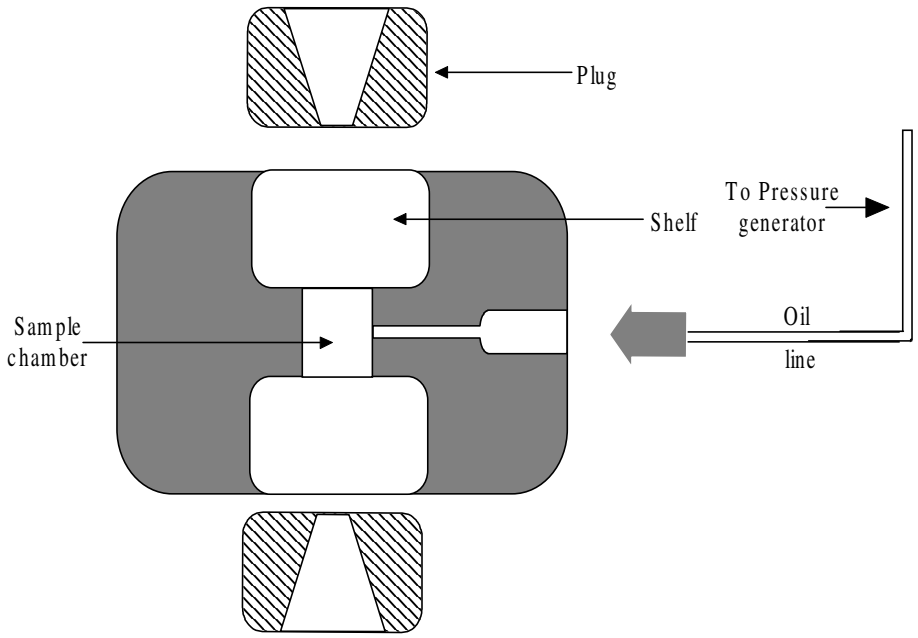

Figure 2.1: Schematic diagram of the basic parts of High Pressure cell

On the inside, the plugs have a small protrusion which are made optically flat by handlapping. These plugs keep the sample assembly in position. The central hole of the upper plug is sealed by a fused quartz cylinder which also forms a part of the sample assembly. The hole in the cell body for the pressure connection consists of two stages: a smaller hole (about 1.2 mm diameter) which extends from the interior of the body to about two-thirds of the thickness (this hole ends in a 60^0 cone taper with a 2 mm opening) and joins a larger hole (1cm in diameter and 1cm in depth) bored from outside.

2.22 Sample Chamber

A schematic representation of the HP optical setup is shown in Figure 2.2. In order to develop high pressure in the small central sample chamber it is essential to have a tight seal along both boundaries of the plugs: one for the central hole and the

other along the circular boundary of the chamber against the plug. The threads of the plug alone are not enough to have a leak proof assembly. A thin clearance between the plug and the sample chamber caused by a slight lifting of the plug by high pressure leads to a leak of the oil to the outside. This leak is avoided by placing a

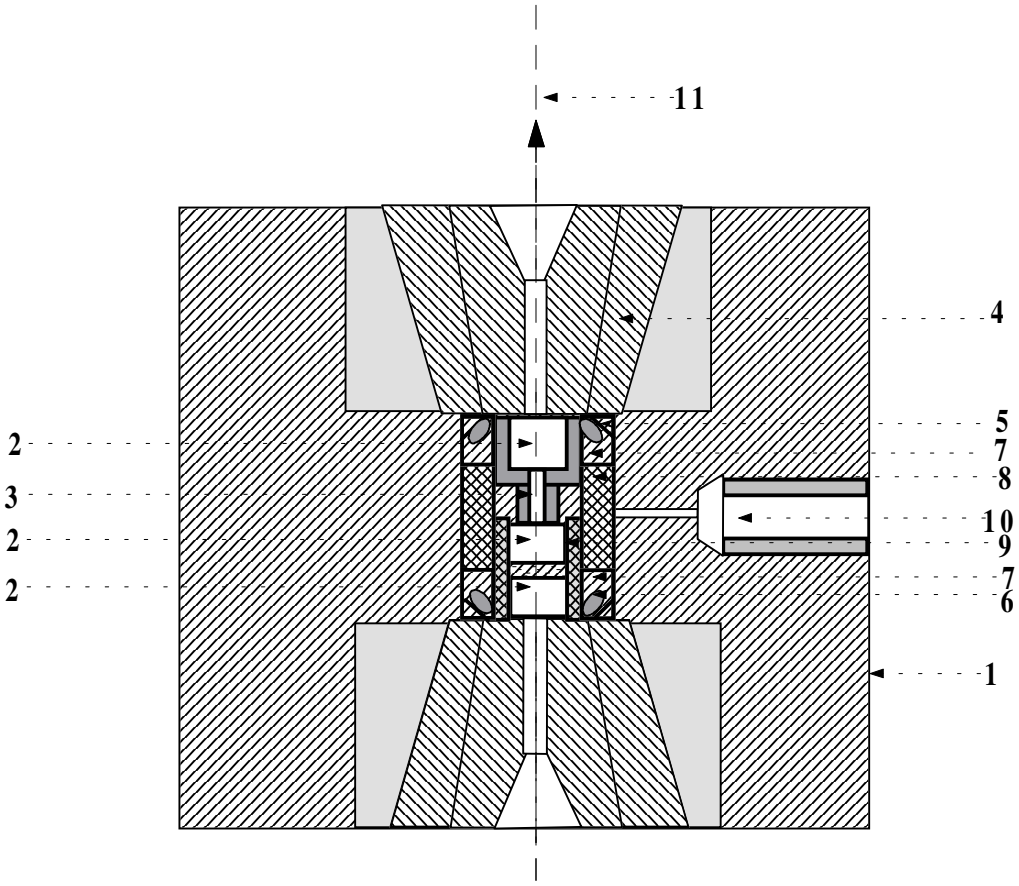

Figure 2.2: Schematic diagram of HP optical cell: 1-Cell body; 2-fused quartz windows; 3-glass rod; 4- steel plug; 5- anti extrusion ring; 6-'O' ring (neoprene); 7-outer spacer; 8-Central spacer; 9-Fluran tube; 10 - HP connection; 11- transmitted light.

neoprene 'O' ring around the junction. As the oil pressure increases, the 'O' ring is pushed to the corner and the seal is made at the point where the 'O' ring touches the cell body. Once the seal is achieved, oil cannot leak out. The only problem is that at a sufficiently high pressure, the 'O' ring itself extrudes through the small gap between the cap and the seating of cell body. This eventual breaking of the seal naturally results in a leak. This problem has been solved by the use of an anti extrusion ring which is a steel ring with triangular cross section. This blocks the extrusion of the 'O' ring, while the 'O' ring keeps oil from leaking out (Figure 2.2). The seal at the central hole of the plug is made with a fused quartz window, so that optical transmission is

not affected. A small washer made of thin aluminium foil fills any crevices on the surface of the plug. A glass rod is placed in the space between the topmost fused quartz and the sample cell (Figure 2.2) to reduce the amount of oil between the two and thereby increasing the intensity of the transmitted light.

2.23 Heating of HP cell

The temperature of liquid crystal phase transitions will significantly increase with increasing pressures. Hence HP studies of liquid crystal transitions require quite high temperatures, ~ 200 ^{0}C. It is necessary to have a heating system which can rise the temperature of the entire HP cell assembly. A schematic representation of the heating assembly is shown in Figure 2.3. The heating system is made of an aluminum cylinder whose internal diameter is such that the pressure cell can be push-fitted into it. Thus it also acts as a binding ring for the pressure cell. Mica is an electrical insulator. Nichrome tape wound on mica sheets is the heating element with a resistance ≈ 37 Ω and the mica strips in turn are wrapped around the inside wall of the aluminium cylinder. The effective heating power is about 120 watts. The required power to heat the system is supplied through the Hewlett- Packard system power supply (hp 6038A; 0-60V/0-10A, 200W). A radial hole made through the aluminium cylinder facilitates to take out the pressure tubings from the pressure cell to the outside.

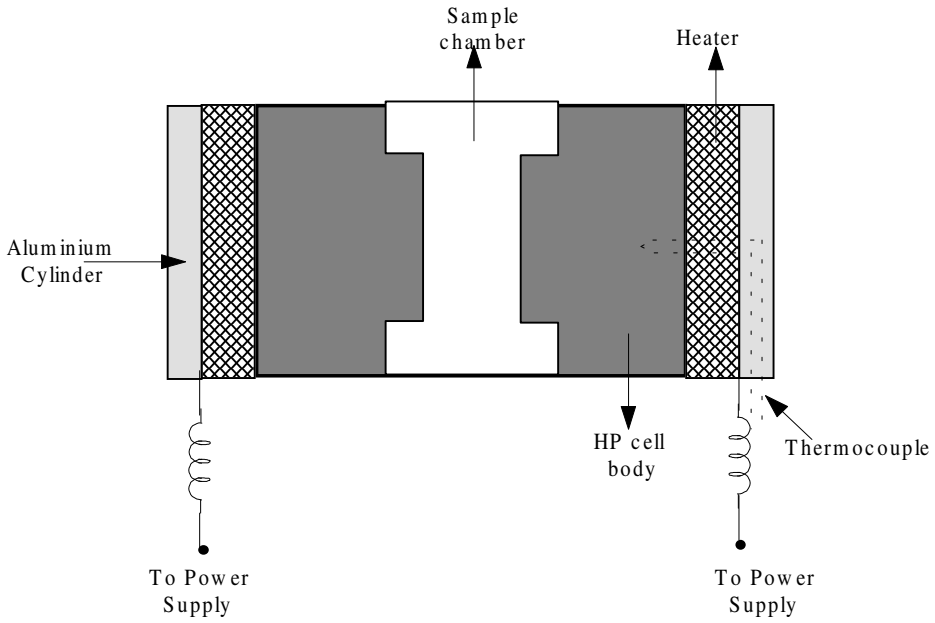

Figure 2.3: Schematic representation of the heating assembly of HP cell.

The temperature sensed by the sample is measured using a Chromel-Alumel thermocouple sheathed in a ceramic tube located such that its junction just touches the cell body. No hole is drilled on the cell body for the insertion of the thermocouple since that would considerably weaken the cell body. There will be a difference in the temperature of the sample and that sensed by the thermocouple junction which can be corrected by calibration of the system using standard samples.

2.24 High Pressure Plumbing System

The Schematic diagram of the HP plumbing system is as shown in Figure 2.4. A hand-pump (PPI, USA) is used to generate the pressure in the cell. Fine variations in pressure can be made using a pressure generator, (HIP, USA) with a small displacement capacity. The line pressure is measured by a Bourdon type (HEISE) gauge. The plumbing connections are made through two-way and three-way valves. The tubing used is made of seamless stainless steel material with inner diameter 2mm and outer diameter 10mm. The tubing as well as the valves can withstand line pressures upto 7 kbar.

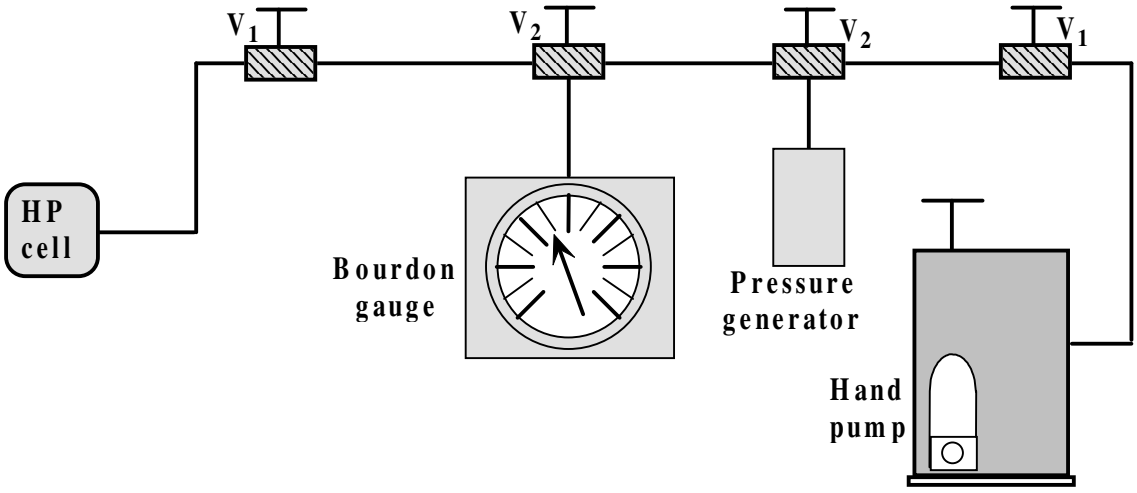

Figure 2.4: Schematic diagram of the HP plumbing system - V_1: two-way valve, V2: three-way valve.

The sample is pressurised by the priming action of a hand-pump. Pulling the handle of the pump raises the piston and draws oil from the reserve into the pump's chamber. Pushing the handle down lowers the piston which compresses the oil and sends it through the steel line into the cell. The pressure at the hand pump was not

holding for long times, possibly due to a slight leak in the pump. Hence each time the line pressure was locked to ensure that the sample experienced a constant pressure. The pressure in the HP cell sensed by the sample is the same as the line pressure. The measured pressure is accurate to ± 2 bars.

2.25 Sample Preparation

The main difficulty in the study of liquid crystals under high pressures is the isolation of the sample from the pressure transmitting medium. In the earlier high pressure optical studies [8] the liquid crystal sample was sandwiched between optically polished sapphire windows which are birefringent. In the optical path difference measurements we use 5mm thick (8 mm diameter) fused quartz cylinders which are optically isotropic. The fused quartz cylinders are coated with polyimide and cured at 280 ^{0}C for about an hour and then unidirectionally rubbed using soft tissue paper. The sandwich is prepared such that the directions of rubbing of both the cylinders are parallel to each other allowing the sample to align homogeneously with the director lying along the rubbing direction. A mylar spacer is used to fix the thickness of the sample. The sandwiched sample is snugly fit into a fluran tube. Fluran is an elastomer which can withstand temperatures upto 300 ^{0}C, and can transmit hydrostatic pressures very well. An effective seal is realised by tightly binding thin steel wires around the tubing on both fused quartz windows. A schematic representation of the sample assembly is shown in figure 2.5.

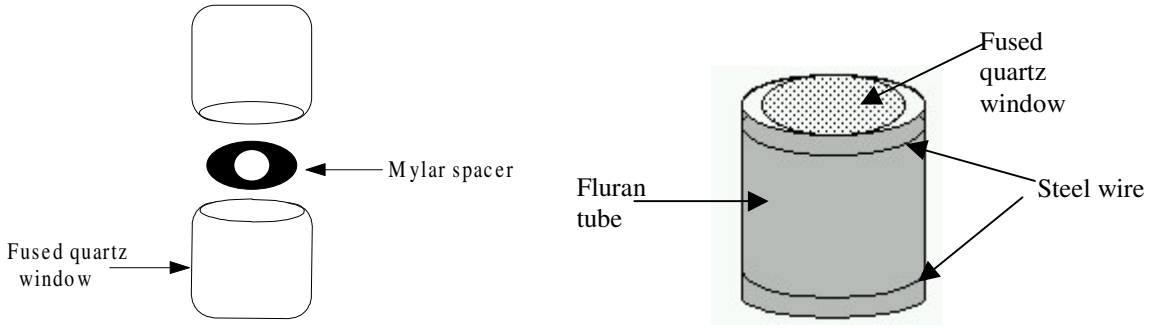

Figure 2.5: Schematic representation of sample cell.

2.26 Modification of High Pressure Optical Setup

We have modified the HP optical setup so that the optical path difference of an aligned sample can be measured. The source intensity fluctuations can be taken into account by monitoring a reference beam to check for the stability of source. A continuous optical beam creates a DC signal at the output of the photodiode. Any perturbation of the signal due to stray light will also be amplified and appear as an output. If the continuous optical beam is converted into an alternating signal the fluctuations caused by stray light can be eliminated by a phase sensitive measurement. A precision Light chopper (EG&G model 198) which is a frequency programmable chopper is used for this purpose. It has two sets of user accessible chopping apertures and another third (non accessible) set of apertures which produce a synchronous frequency equal to the sum of the two chopping frequencies. The inner and outer chopping frequencies and the sum synchronous frequency are in the ratio 11:18:29. These frequencies are chosen to be relative primes so that the mutual harmonic interference can be reduced significantly. To take source intensity fluctuations into account we use a lock-in amplifier (LIA; EG&G model 7260) in the dual reference mode. In this mode, two different optical signals being chopped at two different reference frequencies can be simultaneously measured using a single photodiode. One reference frequency is connected to the relevant external reference input connector of LIA and the second reference is derived from the internal oscillator of LIA. The schematic diagram of the modified HP optical setup is shown in Figure 2.6. A He-Ne laser (Oriel; 3mW) beam of wavelength 633nm is split into two beams using a beam-splitter. The two beams are made to pass through the two different windows of the same chopper (EG&G model 198). We have chosen the sum frequency of chopper to be 1000Hz. The beam passing through the chopper window operating at 379Hz passes through the sample placed between crossed polarisers which are mounted on rotatable graduated discs. The beam passing through the other window operating at 621Hz is used as the reference beam. Both the beams are combined at a beam-combiner and detected using a single photodiode (Hamamatsu S1406, with a built-in amplifier). The photodiode output is measured using LIA in dual reference mode. The ratio of the intensity of the beam transmitted through the sample (I_{tr}) to that of the reference beam (I_{ref}) is used in the further processing of data.

We also use a microscope to observe the textural changes in the sample and the schematic diagram of the setup is shown in Figure 2.7.

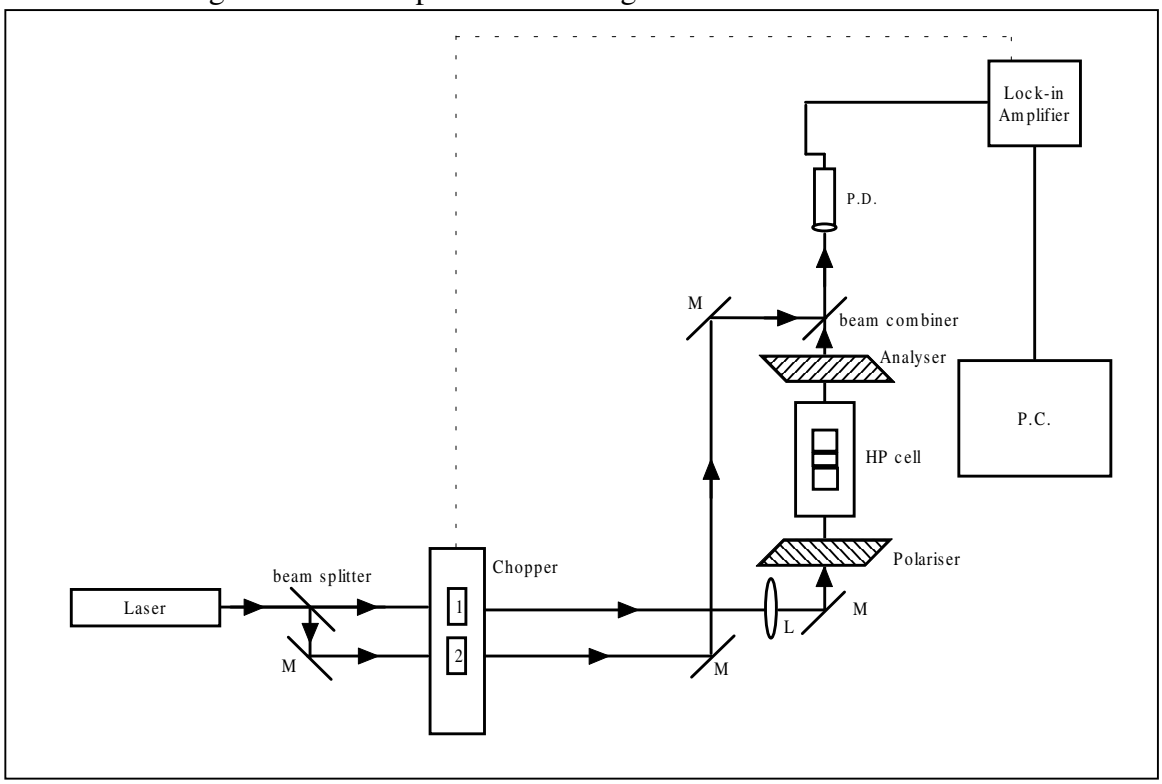

Figure 2.6: Schematic diagram of the modified high pressure optical setup: M-mirror, L-lens, P.D. – photodiode, P.C.-personal computer

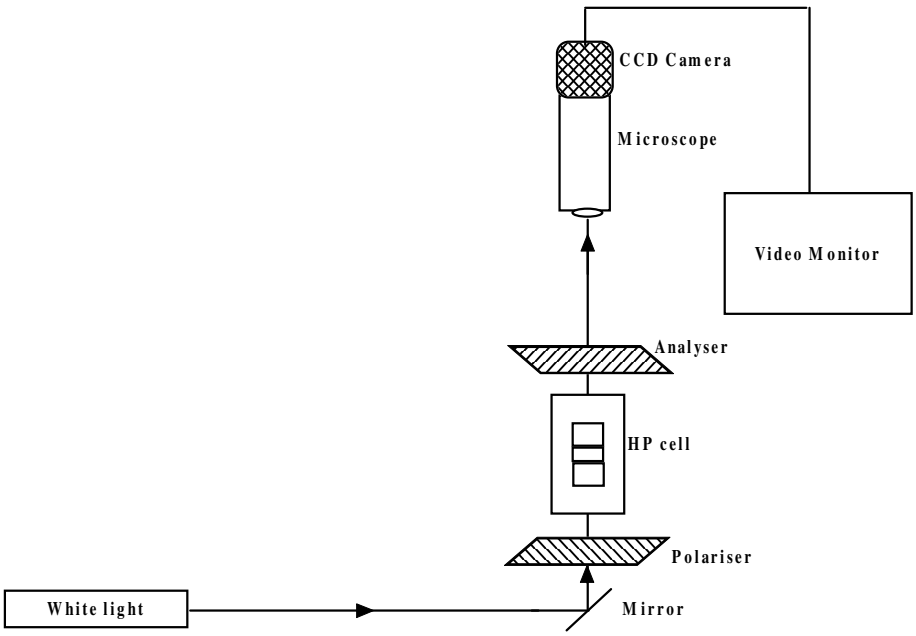

Figure 2.7: Schematic representation of the HP optical setup for the observation of mesophase textures.

A photograph of the modified HP optical setup is presented in Figure 2.8. A more detailed view of the components of the setup is presented in Figure 2.9.

Figure 2.8: Photograph of the modified High Pressure Optical setup.

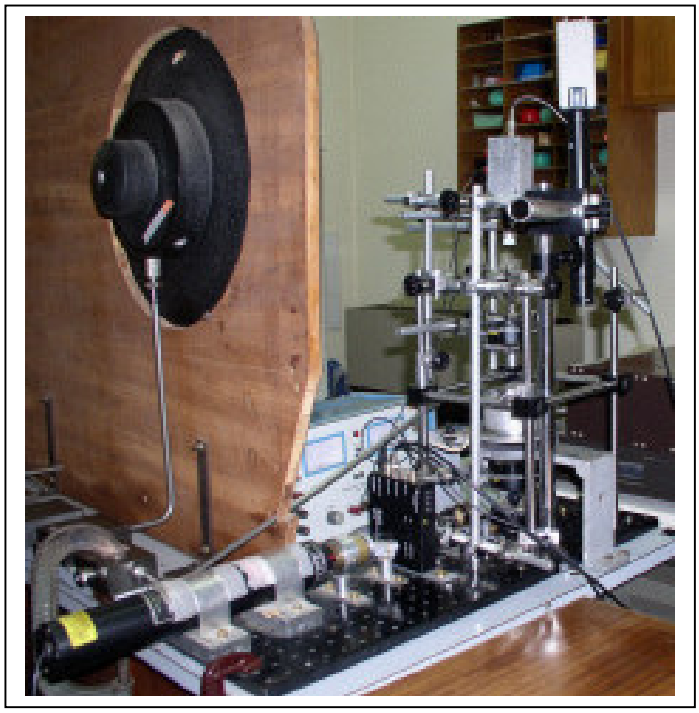

Figure 2.9: A close-up photograph of the modified High Pressure optical setup showing all the optical components.

2.27 Temperature Control and Intensity Measurement

One of the junctions of Chromel – Alumel thermocouple has to be maintained at 0 ^{0}C which is usually done by using ice filled in a thermos flask. We have used a temperature controller (fabricated at the National Aerospace Laboratory) which has a built in room temperature compensation for the cold junction of the thermocouple. The sample temperature can be controlled to an accuracy of 25 mK. A Software program is used to control the temperature and record the transmitted intensity signals at various temperatures. A schematic representation of the flow chart of program is shown in Figure 2.10. In this program the Proportional, Integral and Derivative (PID) concept is used to control the temperature. The power at a given instant of time P(i) to be supplied to the heater is given by $P(i) = \alpha [\Delta_i + \beta \sum_{j<i} \Delta_i + \gamma(\Delta_i - \Delta_{i-1})]$, where $\Delta_i = \{A(Ttemp - Mtemp)\}$ at a given instant of time. Ttemp and Mtemp are the target temperature and measured temperature respectively. The PID parameters α,β,γ and constant factor A are chosen by trial and error for optimal working conditions. All the instruments are interfaced to a PC (Personal Computer) through an IEEE - 488 general purpose- interface bus (GPIB) card.

The meanings of the terms used in the program are as follows: Fname: Name of the file in which the data has to be stored, Stemp: Starting temperature, Ttemp: Target temperature, Etemp: End temperature, Mtemp: measured temperature, Tstep: temperature step by which temperature has to be incremented or decremented, Ptemp: Post experiment temperature i.e. temperature at which the system has to be held once the experimental run is complete, stab: temperature stability required, Htime: Time in seconds for which the sample has to be held at any given target temperature to a given accuracy. {T, T_0, T_1}: Time in seconds, rms: root mean square deviation error from target temperature (rms = $\sum_{j=i-50}^{i} \sqrt{(\Delta temp_i)^2/50}$), where $\Delta temp_i$ = Ttemp – Mtemp. I_1, I_2 are the intensities measured by LIA in the dual reference mode, R: ratio of the transmitted intensity through the sample (I_1) to the reference intensity (I_2). Each time a reading is taken, automatically the sensitivity of the LIA is set using the 'autosensitivity' command. At any stage of the program a change can be made by pressing one of the following keys: 'Esc' or 'Ctrl + Break'. On pressing 'Esc' key, the power supplied to the system remains the same till another

program is executed. Pressing the 'Ctrl + Break' the power supply switches off automatically.

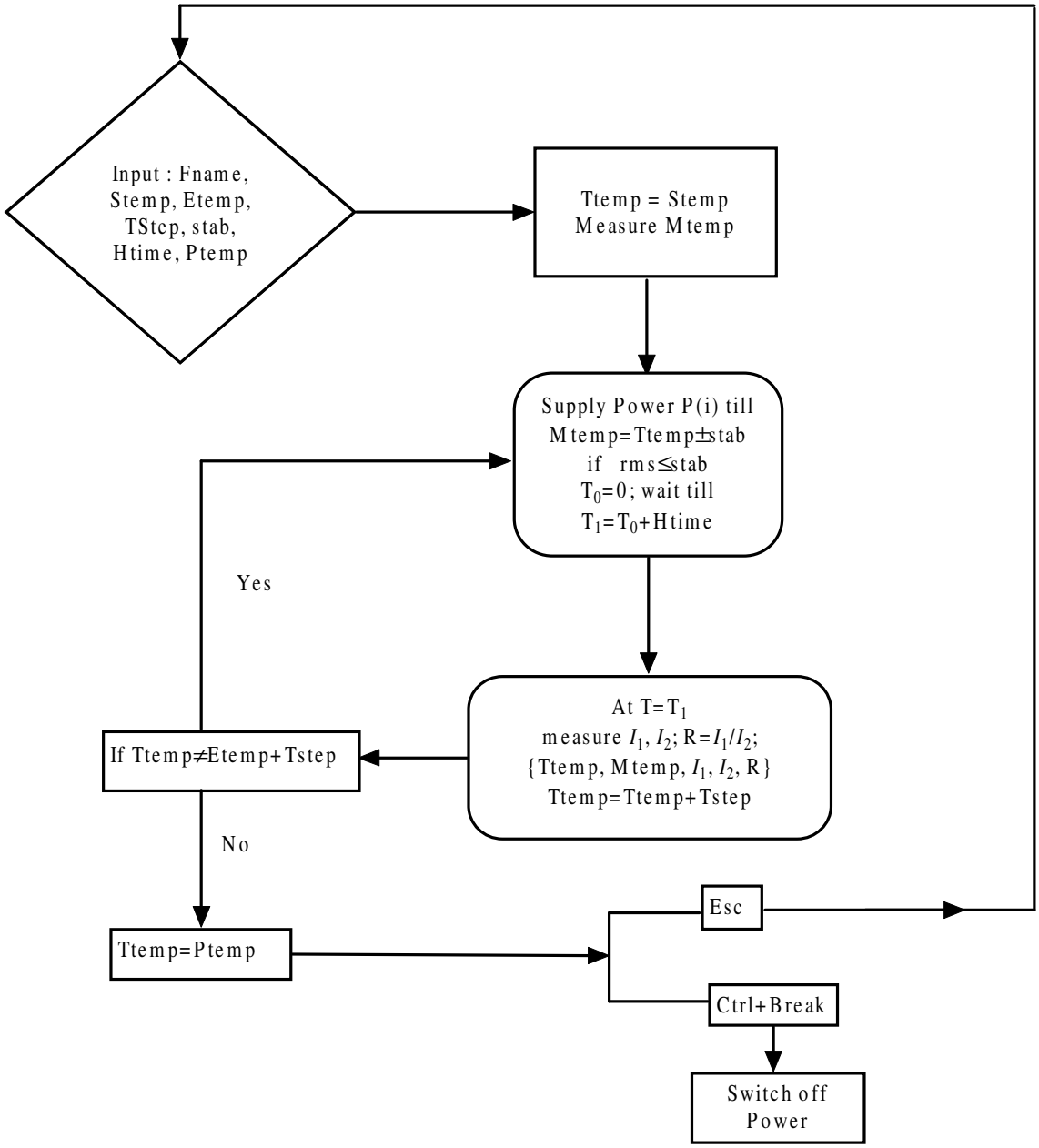

Figure 2.10: Schematic representation of flow chart of program used to control temperature as well as record intensities at each temperature step.

2.28 Experimental Method

The orientation of polarisation of the laser beam was found to change with time. This causes problems in measurement, as the source beam is split into reference and sample beams which pass through two different optical paths (Figure 2.6). The problem is avoided by allowing the laser beam to pass through a crystal polariser (Figure 2.9), whose orientation is adjusted such that the intensity of the beam passing through the sample is maximum. To make path difference measurements it is essential to know the optic axis decided by the rubbing direction of the sample. The HP cell is fixed onto a rigid base and cannot be rotated to identify the rubbing direction of the sample. Hence the crossed polarisers (Figure 2.6) are rotated in tandem and the orientation of rubbing direction is identified by a minimum in transmitted intensity. This orientation corresponds to that at which the rubbing direction of the sample is parallel to one of the crossed polarisers. The polariser and analyser are then rotated by 45^0 in tandem from the orientation corresponding to minimum intensity. This setting corresponds to the one of maximum sensitivity.

In this geometry the transmitted intensity is given by

$$I_{tr} = I_0(1-\cos\Delta\phi)/2 \qquad (2.1)$$

I_0 corresponds to the intensity of the polarised beam entering the sample. $\Delta\phi$ is the optical phase difference given by

$$\Delta\phi = 2\pi t\Delta\mu/\lambda \qquad (2.2)$$

and $\Delta\mu = \mu_e - \mu_o$, where μ_e and μ_o are the two principal refractive indices of the medium, t the sample thickness and λ the wavelength of the incident light (633nm). The sample is heated to the isotropic phase and the analyser is rotated such that it is parallel to the polariser and the intensity I_0 is noted down. Again analyser is rotated back to the previous orientation such that it is crossed with respect to the polariser.

The profile of ratio of transmitted intensity to reference intensity on cooling the sample in equal temperature steps (~ $0.1\ ^0$C or $0.2\ ^0$C) at various fixed pressures are recorded from the isotropic phase down to appropriate temperatures using the automated temperature control program. Data of a typical experimental run is shown

in Figure 2.11. The isotropic to nematic transition is characterised by a sharp jump in the intensity reflecting the first order nature of the transition. The value of $\Delta\mu \propto S$ increases with decreasing temperature. The transmitted intensity is an oscillatory function (equation 2.1) with maxima and minima occurring for $\Delta\phi=(2m+1)\pi$ and $2m\pi$ respectively, where m is an integer. The rate of increase of $\Delta\mu$ with decreasing temperature also decreases, and the consecutive maxima and minima get broadened with lowering of temperature. As seen in Figure 2.11 the value of the measured transmitted intensity is zero in the isotropic phase as expected. The values of transmitted intensities at the minima in the nematic phase are also expected to be zero (equation 2.1). But as seen in Figure 2.11 the minima have finite values of intensity. This implies that the value of $\Delta\phi$ at the minima has a spread around $2m\pi$. This indicates that the thickness has a gradient in the sample area ~ 5 mm^2 illuminated by the laser beam. As discussed earlier the thickness of the sample cell is fixed by using a mylar spacer cut in circular shape and not sealed using any glue. This technique can result in a non uniform thickness.

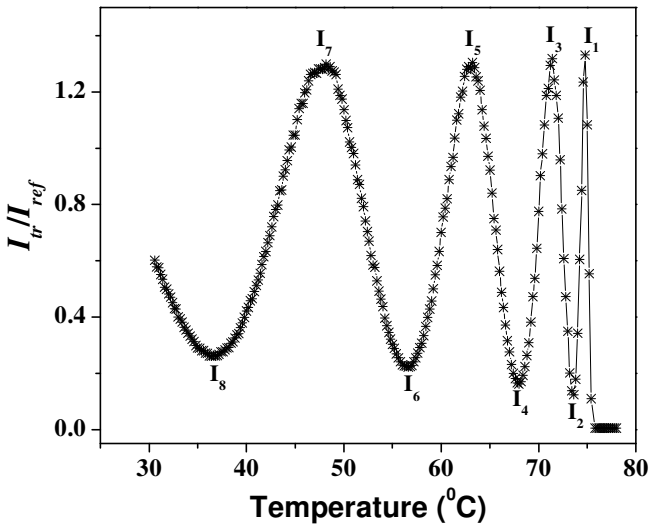

Figure 2.11: The temperature variation of the ratio of transmitted intensity to reference intensity of 20.4 μm thick sample of 6OCB (hexyloxy cyanobiphenyl) at atmospheric pressure.

2.29 Estimation of birefringence, $\Delta\mu$

Method 1:

Assuming a linear gradient in thickness, i.e. the thickness t varies from t - Δt to t + Δt and using equations 2.1 and 2.2, the transmitted intensity averaged over thickness t - Δt to t + Δt is given by

$$\bar{I}_{tr} = I_0\left[1 - \overline{\cos(2\pi t\Delta\mu/\lambda)}\right]/2 \qquad 2.3$$

where $$\overline{\cos(2\pi t\Delta\mu/\lambda)} = \int_{t-\Delta t}^{t+\Delta t}[\cos(2\pi t\Delta\mu/\lambda)]dt \Big/ \int_{t-\Delta t}^{t+\Delta t} dt \qquad 2.4$$

Equation 2.3 can be written as

$$\bar{I}_{tr} = \frac{I_0}{2}\left[1 - \left\{[\cos(2\pi t\Delta\mu/\lambda)]\frac{[\sin(2\pi\Delta t\Delta\mu/\lambda)]}{(2\pi\Delta t\Delta\mu/\lambda)}\right\}\right] \qquad 2.5$$

Using the values of $\Delta\mu$ of 6OCB available in the literature [20] corresponding to temperatures at which a few maxima and minima occur, the integer m and hence the average thickness of sample t = 20.4 μm are estimated. The variations of $\bar{I}_{tr}/I_0$ with $\Delta\mu$ for various values of Δt using equation 2.5 with average thickness t = 20.4 μm are shown in Figure 2.12.

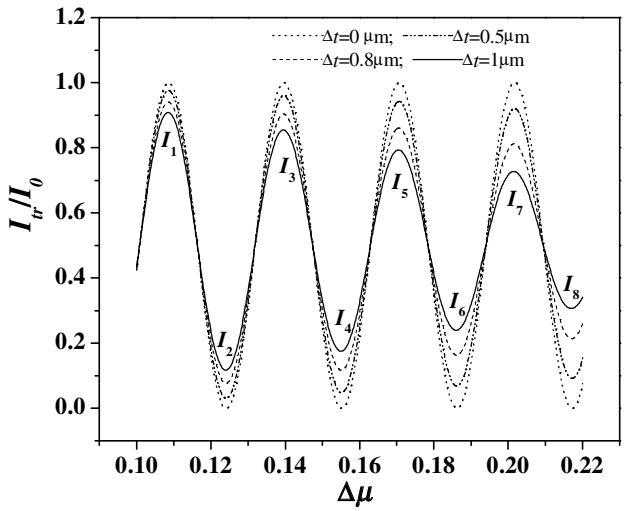

Figure 2.12: The calculated profiles of $\bar{I}_{tr}/I_0$ as a function of birefringence $\Delta\mu$ for various values of Δt.

As seen from Figure 2.12 the values of $\bar{I}_{tr}/I_0$ at maximum (minimum) decrease (increase) considerably for Δt = 1μm compared to those for Δt = 0. But the values of $\Delta\mu$ at which maxima and minima occur decrease only by ~ 0.1% for Δt = 1 μm compared to those for Δt = 0. This is due to the fact that in equation 2.5, the *sinc* function viz. $[\sin(2\pi\Delta t\Delta\mu/\lambda)]/(2\pi\Delta t\Delta\mu/\lambda)]$ varies very slowly with $\Delta\mu$ even for a value of Δt =1μm. For any particular finite Δt the values of $\bar{I}_{tr}/I_0$ at successive maxima decrease with increasing $\Delta\mu$, whereas the $\bar{I}_{tr}/I_0$ values at minima increase with increasing $\Delta\mu$. The ratio of $\bar{I}_{tr}/I_0$ at a given maximum to that at the successive minimum calculated for a few values of Δt are presented in Table 1. We have also given the relevant experimental results. As the intensity is recorded for temperature steps of 0.2 ^{0}C, the true maxima and minima may not be located in the experiment, especially for the first maximum. Hence I_1/I_2 of experimentally recorded intensity profile may be underestimated.

Δt (μm)	I_1/I_2	I_3/I_4	I_5/I_6	I_7/I_8
0.74	14.2	9.0	6.2	4.5
0.76	13.5	8.5	5.9	4.2
0.78	12.8	8.1	5.5	4.0
0.80	12.2	7.7	5.3	3.8
exptal	10.8	8.1	5.9	4.8

Table 1: Table of ratios of $\bar{I}_{tr}/I_0$ at a given maximum to that at the successive minimum calculated for a few values of Δt (the last row denoted as exptal corresponds to the intensity profile shown in Figure 2.11).

As shown in Table 1 there is a reasonable agreement between experimental data and calculated data for $\Delta t \approx 0.76$ μm. The values of $\Delta\mu$ are now calculated from the intensity data using equation 2.5 with 19.64 μm ≤ t ≤ 21.16 μm.

Method 2:

We have estimated the values of $\Delta\mu$ using another simple method. We assume that the value of $I_0 = I_{max} - I_{min}$ where I_{max} and I_{min} are the values of the transmitted intensities at the maximum and minimum of the corresponding branch in the oscillating intensity profile. I_{tr} at a given temperature is assumed to be $=I_{meas} - I_{min}$, where I_{meas} is the transmitted intensity measured at any given temperature. Making use of the value of average sample thickness t=20.4 μm, the temperature variation of $\Delta\mu$ is estimated using equations 2.1 and 2.2. The estimated values of $\Delta\mu$ using this procedure for temperatures upto $T_{NI} - T = 2\ ^0$C are lower by <1.3% compared to the values estimated using the first method in which the gradient in thickness is taken into account. At lower temperatures, values of $\Delta\mu$ calculated using both the methods are in very good agreement as shown in Figure 2.13. For simplicity, we employ the simpler method in all further calculations of $\Delta\mu$ from the intensity data.

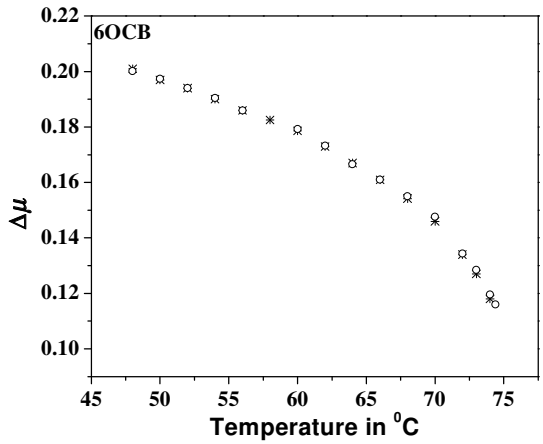

Figure 2.13: The temperature variation of birefringence $\Delta\mu$ of 6OCB estimated using both methods (o- corresponds to the first method where in a gradient in thickness Δt is taken into account ; ✳ corresponds to the second method).

2. 3 Results and Discussion

2.31 Temperature Calibration of the HP system

The temperature controller reads the temperature in ^{0}C. We have conducted HP optical phase difference measurements on the liquid crystal compounds listed below. The mesophase transition temperatures of these compounds at atmospheric pressure are determined using a hot-stage (Mettler FP 82). The temperature of the HP system is calibrated by comparing the transition temperatures measured at atmospheric pressure with those measured using hot-stage.

The mesogens used in the study are: (i) 4-hexyloxy 4′-cyanobiphenyl (6OCB), (ii) 4-octyloxy 4′ -cyanobiphenyl (8OCB) (iii) 2-cyano 4-heptylphenyl 4′-pentyl-4-biphenyl carboxylate [(7(CN)5)] (iv) p-cyanophenyl p-n hexylbenzoate CP6B (v) p-cyanophenyl p-n heptylbenzoate (CP7B) (vi) 4-(2′-methyl butyl) phenyl 4′-n-octylbiphenyl-4-carboxylate (CE8), which is a chiral compound. The first three compounds were obtained from Messrs. Merck. CP6B and CP7B were obtained from Messrs F. Hoffmann –La Roche & Co. Limited and CE8 from Messrs. BDH Limited.

Liquid Crystal Compounds	Transition	T_S in ^{0}C (Mettler FP82) hot-stage	T_m in ^{0}C (thermocouple in the HP setup)
CP6B	Nematic- Isotropic	47.7	50.0
CP7B	Nematic- Isotropic	56.5	58.5
6OCB	Nematic- Isotropic	74.6	76.4
8OCB	Smectic A - Nematic	67.2	69.0
8OCB	Nematic- Isotropic	80.2	81.8
[7(CN)5]	Nematic- Isotropic	102.7	103.8
CE8	Blue phase - Isotropic	141.0	142.2

Table 2: List of liquid crystal compounds and the mesophase transitions, transition temperatures of mesophases measured using Mettler (FP 82) as well as the thermocouple in the HP setup at atmospheric pressure.

All the above compounds are chemically stable compounds. The mesophase transition temperatures at atmospheric pressure observed using HP optical setup (T_m) as well as measured using Mettler hotstage (T_s) are listed in Table 2. The plot of T_m as a function of T_s is shown in Figure 2.14. The values of slope as well as the intercept obtained using a linear square fit of the data to a straight line are 0.988 and 2.6 ^{0}C respectively. As mentioned in section 2.23 the thermocouple used to measure the temperature sensed by the sample is situated such that it just touches the cell body. Hence, the temperature measured using HP optical setup is ~2 ^{0}C larger compared to the value of temperature measured using hot-stage.

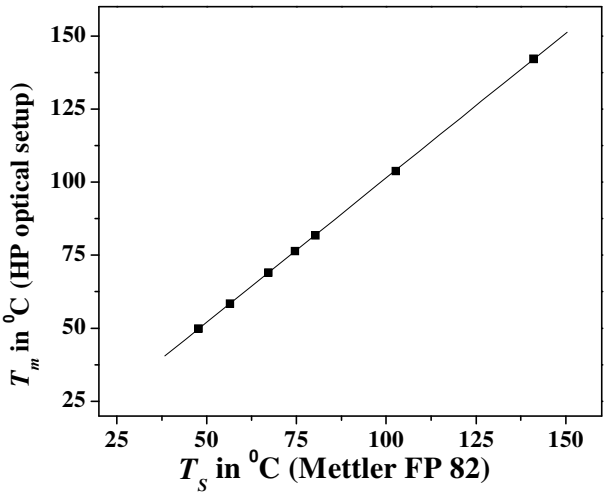

Figure 2.14: The transition temperature observed using HP optical setup (T_m) at atmospheric pressure as a function of temperature measured using Mettler (FP 82) hotstage (T_s).

2.32 Pressure Calibration of the HP system

We conducted HP studies on 8OCB, whose P-T phase behaviour [21,22] is well established. 8OCB exhibits re-entrant Nematic phase (N_r) at elevated pressures. The measurements were carried out on both increasing and decreasing pressure and it was found that the transition temperature at any pressure was independent of the pressure cycling. For pressures above 1.1 kbar, T_{NI} shifts beyond 120 ^{0}C and the measurements were made only to detect the SmA_d - N and N_r - SmA_d transition temperatures. The P-T phase diagram of 8OCB is shown in Figure 2.15a in which the transition temperatures corresponding to N-I, SmA_d - N and N_r - SmA_d transitions

are plotted as functions of pressure. Cladis et al [22] have conducted the HP measurements on three samples of 8OCB of different purity. Though the qualitative aspects of the P-T curves are similar for all three samples of 8OCB, quantitatively they differ in the values of P_m, the maximum pressure at which the SmA_d phase gets bound as shown in Figure 2.15a. The purest compound shows $P_m \approx 2.3$ kbars whereas for the least pure compound $P_m \approx 1.6$ kbars. It can be noticed that our measurements are closer to the data on the purest sample. From our measurements $P_m \approx 2.15$ kbar. The value of $dP/dT_{NI} = 30$ bar/^{0}C compares with the value of $dP/dT_{NI} = 30.2$ bar/^{0}C obtained by Cladis et al [22].

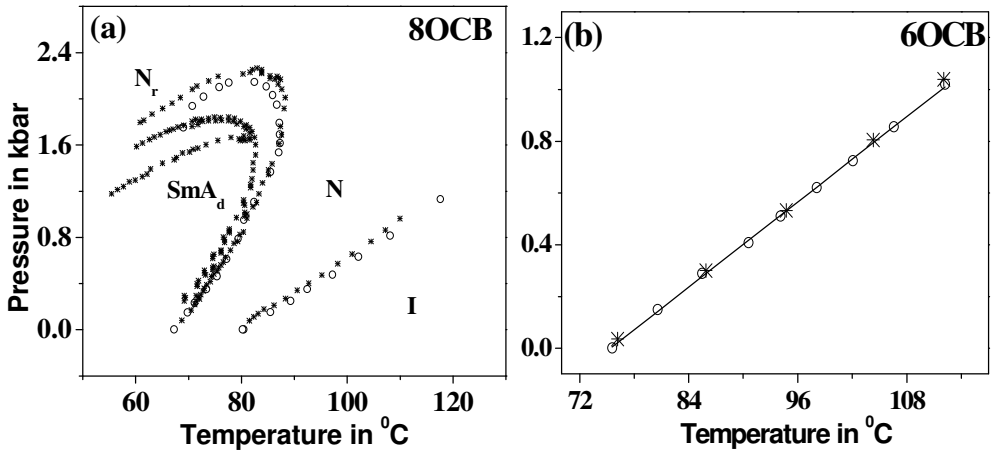

Figure 2.15: The P-T phase diagrams of (a) 8OCB (○ and ✳ correspond to data from our measurements and reference [22] respectively) (b) 6OCB (○ and ✳ correspond to data from our measurements and reference [23] respectively).

We have also conducted HP measurements on 6OCB. The phase diagram of 6OCB in which T_{NI} is plotted as a function of pressure matches well with the one reported by Krombach and Schneider [23] as shown in Figure 2.15b. The value of $dP/dT_{NI} = 27.5$ bar/^{0}C got from our measurements agrees with $dP/dT_{NI} = 27.9$ bar/^{0}C obtained by Krombach and Schneider [23] .

2.33 Estimation of Order parameter (*S*)

The birefringence $\Delta\mu$ is estimated as a function of temperature from the transmitted intensity profile for any given compound using the method explained earlier for 6OCB.

To a good approximation the orientational order parameter $S \approx \Delta\mu/\Delta\mu_0$, where $\Delta\mu_0$ is the birefringence value for the medium with perfect orientational order ($S = 1$). The temperature variation of S can be fitted to Haller's extrapolation formula [24], viz.

$$S = (1 - T/T^{\dagger})^{\beta} \qquad 2.6$$

where $T^{\dagger}$ is a temperature at which the S would have smoothly reduced to zero if it did not jump to zero at the slightly lower first order transition temperature T_{NI}, and β is a constant. We have fitted the $\Delta\mu$ values of a given compound at atmospheric pressure to this formula and estimated the value of $\Delta\mu_0$ which is used in the calculation of S values.

The temperature variation of $\Delta\mu$ at ambient pressure for 6OCB is in good agreement (to <1%) with the values reported by Bunning and co-workers [20] as shown in Figure 2.16a. The temperature variation of S at atmospheric pressure estimated using Haller's method for 6OCB matches (to ±1.5%) with that obtained using NMR measurements by Dong and Ravindranath [25] as shown in Figure 2.16b.

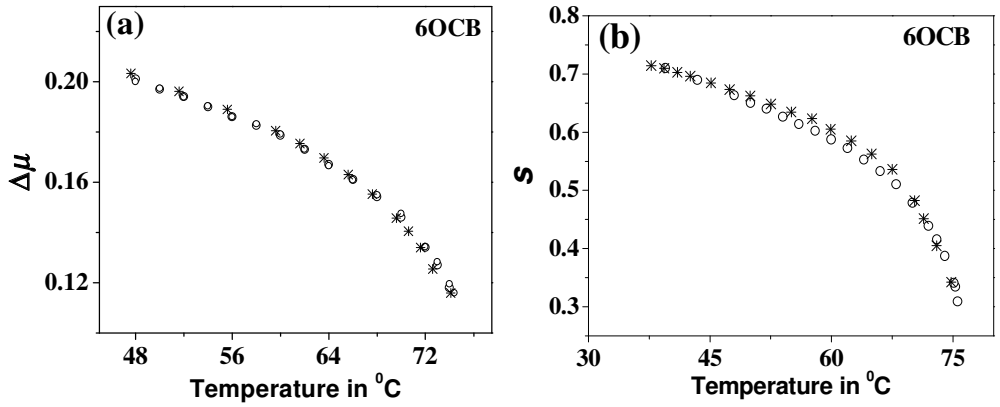

Figure 2.16: Temperature variation of (a) the birefringence $\Delta\mu$ (○ and ✳ correspond to data from our measurements and reference [20] respectively), (b) the orientational order parameter S of 6OCB at atmospheric pressure (○ and ✳ correspond to data from our measurements and NMR data from reference [25] respectively).

Assuming that the sample thickness t remains the same on application of high pressures, the temperature variation of $\Delta\mu$ is estimated along the various isobars using the intensity data. The value of $\Delta\mu_0$ estimated from the atmospheric pressure data is used in the calculation of temperature variation of S at various pressures.

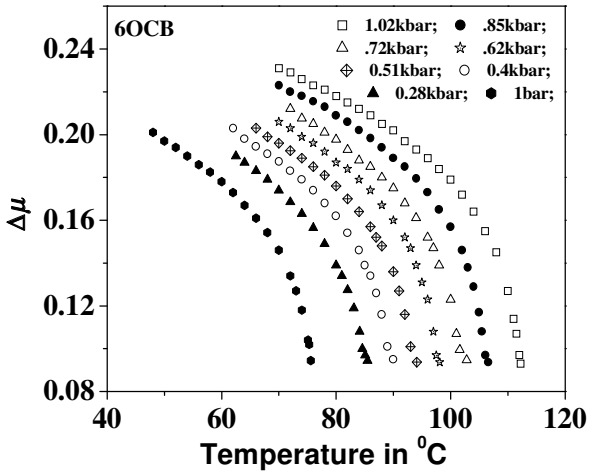

Figure 2.17: Temperature variations of the birefringence $\Delta\mu$ of 6OCB at various pressures.

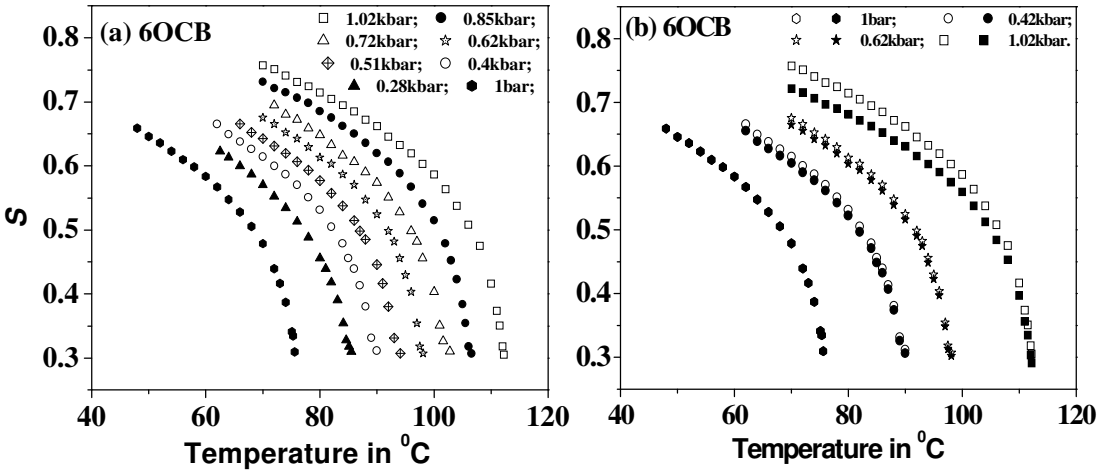

Figure 2.18: Temperature variations of the orientational order parameter S of 6OCB at various pressures estimated (a) using the value of $\Delta\mu_0$ estimated from atmospheric pressure data, (b) open symbols correspond to Figure a, filled symbols correspond to S estimated using the values of $\Delta\mu_0$ along each isobar as shown in Table 3.

The variation of $\Delta\mu$ as function of temperature estimated for 6OCB along various isobars is presented in Figure 2.17. The temperature variation of S for various isobars estimated using the value of $\Delta\mu_0$ estimated from atmospheric pressure data is shown in Figure 2.18a. The value at the NI transition point, i.e., S_{NI} is practically *constant,* and equal to 0.3 (± 1.5%) at all the applied pressures.

The temperature variation of $\Delta\mu$ of 6OCB along each isobar is also fitted to Haller's extrapolation formula. The values of T_{NI}, T^* , the exponent β and $\Delta\mu_0$ are tabulated in Table 3. The value of T^*-T_{NI} decreases with increasing pressure from 1 ^{0}C at P = 1 bar to ≈ 0.6 ^{0}C at P = 1.02 kbar. The value of $\Delta\mu_0$ increases slightly from 0.31 to 0.32 with increasing pressure, whereas the exponent β varies from 0.21 to 0.23. The temperature variations of S for various isobars estimated using the $\Delta\mu_0$ values listed in Table 3 are also shown in Figure 2.18b. It can be seen that the values of S estimated using both methods at pressures upto 620 bars match with each other. At 1.02 kbar the temperature variation of S obtained using the value of $\Delta\mu_0$ calculated along that isobar is lower by ~5% compared to the one estimated using the value of $\Delta\mu_0$ estimated for 1bar. The estimated S_{NI} is constant at all applied high pressures and is equal to 0.3 (± 1.8%).

Pressure In bars	T_{NI} (K)	T^* (K)	β	$\Delta\mu_0$
1	349.5	350.5	0.22	0.31
289	358.5	359.4	0.23	0.31
400	362.6	363.5	0.22	0.31
510	366.2	367.1	0.21	0.31
620	370.6	371.3	0.21	0.31
720	374.6	375.3	0.21	0.32
850	379.1	379.7	0.21	0.32
1020	385.2	385.8	0.22	0.32

Table 3: The table of estimated values of T^*, the exponent β and $\Delta\mu_0$ for 6OCB at various pressures estimated using Haller's extrapolation formula.

The NMR measurements at high pressures on Paraazoxyanisole (PAA) by Deloche et al [13] show that S_{NI} is constant at all applied pressures. Wallis et al [15]

have also found that the values of S_{NI} remain constant for several (but not all) nematogens at different pressures. Indeed the mean field theories such as the Maier-Saupe theory and the one outlined by Deloche *et al* of N-I transition [13] predict that the value of S_{NI} should be independent of pressure along the transition line.

Urban has measured both the dielectric constants $\varepsilon_{\parallel}$ and $\varepsilon_{\perp}$ for 6OCB as functions of pressure along various isotherms [19]. The increase in dielectric anisotropy $\Delta\varepsilon$ with increasing pressure is slower along any isotherm compared to the increase in $\Delta\mu$. They have not estimated the value of S. For compounds with the highly polar cyano end group $\Delta\varepsilon$ is essentially $\propto \rho S/T$ where ρ is the density of the medium. Further, with increasing pressures the density increases, and there is a possibility of change in short range and the dielectric anisotropy can be sensitive to this factor. Hence this data cannot be used for comparison with our measurements of S.

The temperature variation of $\Delta\mu$ of 8OCB at atmospheric pressure matches (to ~2%) with the values reported by Lim and Ho [26] as well as Karat [27] as shown in Figure 2.19a. The estimated values of S at atmospheric pressure for 8OCB are in agreement with the S values reported by Prasad and Venugopalan [28] (based on IR, Raman and $\Delta\mu$ measurements) as shown in Figure 2.19b.

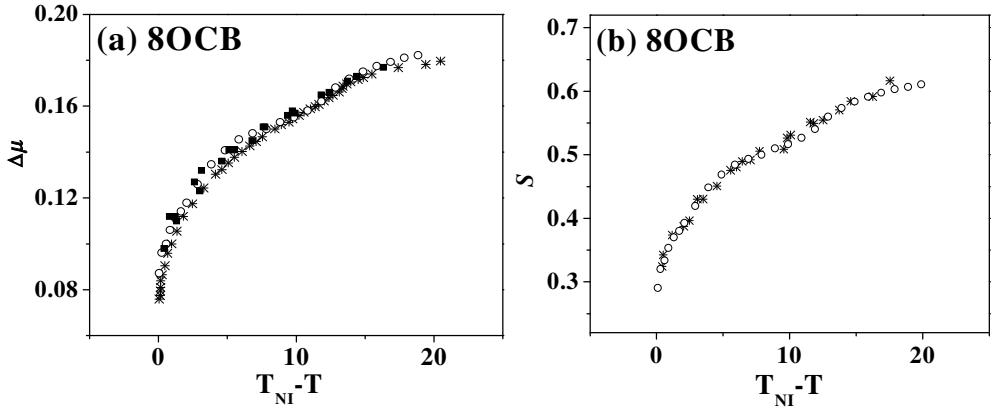

Figure 2.19: Temperature variation of (a) the birefringence $\Delta\mu$ (○ and ✳,■ correspond to data from our measurements and references [26, 27] respectively),
(b) the orientational order parameter S of 8OCB at atmospheric pressure (✳ and ○ correspond to data from our measurements and references [28] respectively).

The temperature variations of $\Delta\mu$ in both nematic as well as smectic A phase of 8OCB at various pressures are shown in Figure 2.20. The variations of *S* as function of temperature at various pressures are shown in Figure 2.21, in which S_{NI} = 0.29 (± 2%) at all applied pressures.

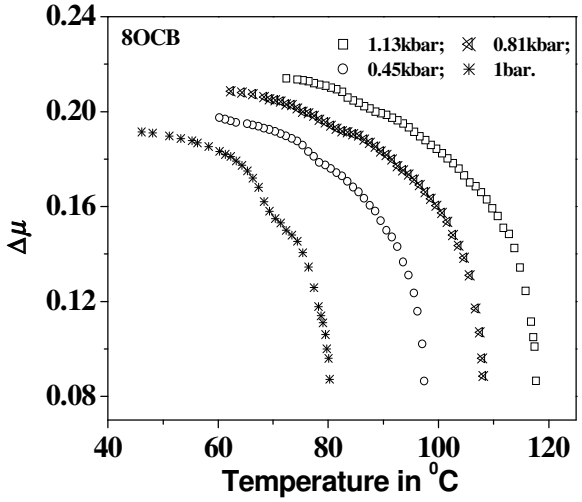

Figure 2.20: Temperature variations of the birefringence $\Delta\mu$ of 8OCB at various pressures.

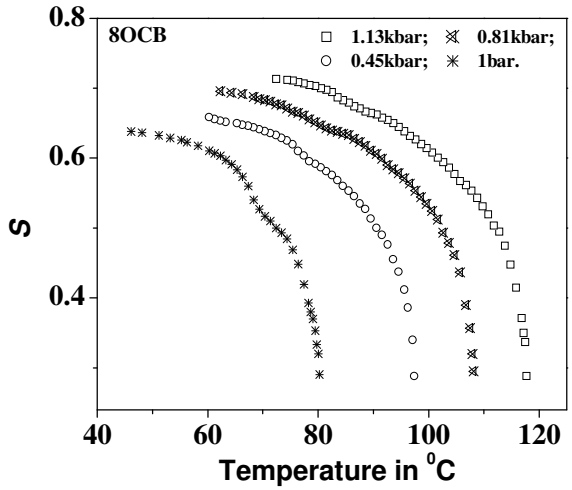

Figure 2.21: Temperature variations of the orientational order parameter *S* of 8OCB at various pressures.

The value of order parameter S at SmA_d - N transition increases with increasing pressure (Figure 2.21). The nematic range increases with increasing pressure as discussed earlier. The strength of SmA_d - N transition becomes weaker with increasing pressure as shown in Figures 2.20 and 2.21. At pressures above 1.6 kbar, SmA_d -N_r phase transition takes place at low temperatures, and the SmA_d phase becomes bounded as shown in Figure 2.15a. For pressures larger than P_m the SmA_d phase is unstable and only the nematic phase exists.

2.4 Conclusions

We have modified the HP optical setup so that the optical path-difference of an aligned sample can be measured as functions of both temperature and pressure. We report the temperature variations of birefringence and hence the orientational order parameter of some liquid crystalline systems exhibiting nematic and smectic A phases. We have found that the order parameter at NI transition is a constant independent of pressure for both the systems reported in this chapter.

References

1. P. Pollmann, "High Pressure Investigations", *Handbook of Liquid crystals*, Ed: D. Demus et al. Wiley-VCH, Weinheim, Vol.**1**. 355-378, 1998.

2. S. Chandrasekhar and R. Shashidhar, "High-pressure studies of liquid crystals", *Advances in Liquid crystals*, Ed: Glenn H. Brown, Academic Press, Vol. **4**, 83-120, 1979.

3. G.A. Hulett, *Z. Phys.chem.* **28**, 629-672, 1899.

4. N.A. Puschin and I. W. Grebenschtschikow, *Z. Phys. Chem. Stochiometrie und Verwandtschaftslehre* (Leipzig) **124**, 270-276, 1926.

5. J. Robberecht, *Bull. Soc. Chim. Belg.* **47**, 597-639, 1938.

6. P.H. Keyes, H.T. Weston and W.B. Daniels, "Tricritical Behavior in Liquid-Crystal System", *Phys. Rev. Lett.* **31**, 628-630, 1973.

7. P.E. Cladis, R.K. Bogardus, W.B. Daniels and G.N. Taylor, "High Pressure Investigation of the Reentrant Nematic-Bilayer-Smectic-A Transition", *Phys. Rev. Lett.* **39**, 720-723, 1977.

8. A.N. Kalkura, R. Shashidhar and N. Subramanya Raj Urs, "High pressure studies on reentrant nematogens", *J.Phys*. **44**, 51-55, 1983; A.N. Kalkura, "High Pressure Optical Studies of Liquid Crystals", *Ph.D. Thesis*, University of Mysore, 1982.

9. P. Pollmann, "Eine Apparatur zur Messung der Lichtreflektion cholesterischer Mesophasen bei hohen Drucken", *J. Phys. E* **7**, 490- 492, 1974.

10. G. Illian , H. Kneppe, F. Schneider, "High Pressure Study on induced S_A phases in binary liquid crystal mixtures" , *Liq. Cryst.* **4**, 643-652, 1989.

11. C. Carboni, H. F. Gleeson, J. W. Goodby and A. J. Slaney, "A specialized apparatus for the study of liquid crystals at high pressures", *Liq. Cryst.* **14**, 1991-2000, 1993.

12. C. Carboni, W.K. Robinson and H.F. Gleeson, "A polarizing microscope for high-pressure studies of liquid crystals", *Meas. Sci. Tecnol.* **4**, 1238-1243, 1993.

13. B. Deloche, B. Cabane and D. Jerome, "Effect of Pressure on the Mesomorphic Transitions in Para-Azoxyanisole (PAA)", *Mol. Cryst. Liq. Cryst*. **15,** 197-209, 1971.

14. J.W. Emsley, G.R. Luckhurst and B.A. Timimi, "The pressure and temperature dependence of the orientational order in nematic phase of 4-n-pentyl-d_{11}-4′-cyanobiphenyl. A deuterium NMR study", *J. Phys*. **48**, 473-483, 1987; J.W. Emsley, G.R. Luckhurst and S.W. Smith, "The pressure and temperature dependence of the orientational order of a biaxial solute dissolved in a nematic solvent", *Mol. Phys.* **70**, 967-984, 1990.

15. G.P. Wallis and S.K. Roy, "Nuclear magnetic resonance studies of liquid crystals under pressure", *J. Phys*. **41**, 1165-1172, 1980.

16. S.Ye. Yakovenko, M. Maiwald, A. Wurflinger and J. Pelzl, " Raman studies of some cyanobiphenyl derivatives under pressure", *Liq. Cryst*. **26**, 23-30, 1999.

17. R.G. Horn, "High pressure measurements of the refractive indices of two nematic liquid crystals", *J. de. Phys*. **39,** 167-172, 1978; R.G. Horn and T.E. Faber, "Molecular alignment in nematic liquid crystals: a comparison between the results of experiments at high pressure and predictions based on mean field theories", *Proc. R. Soc. Lond*. **368A**, 199-223, 1979.

18. S. Urban and A. Wurflinger, "Dielectric Properties of Liquid Crystals under High pressure", *Adv. Chem. Phys*. **98**, 143-216, 1997.

19. S. Urban, "Dielectric Studies of 4-n-Hexyloxy-4′-cyanobiphenyl (6OCB) at Elevated Pressure", *Z. Naturforsch*. **54a**, 365-369, 1999; S. Urban, J. Kedzierski and R.Dabrowski, "Analysis of the Dielectric Anisotropy of Typical Nematics with the Aid of the Maier-Meier Equations", *Z. Naturforsch*. **55a**, 449-456, 2000.

20. J. D. Bunning, D. A. Crellin and T.E. Faber, "The effect of molecular biaxiality on the bulk properties of some nematic liquid crystals", *Liq. Cryst*. **1**, 37-51, 1986.

21. P. E. Cladis, D. Guillon, F. R. Bouchet and P. L. Finn, "Reentrant nematic transitions in cyano-octyloxybiphenyl (8OCB)" *Phys. Rev. A*. **23**, 2594-2601, 1981.

22. P.E. Cladis, R.K. Bogardus and D. Aadsen, "High-pressure investigation of the reentrant nematic bilayer smectic-A transition", *Phys. Rev. A* **18**, 2292-2306, 1978.

23. R. Krombach and G.M. Schneider, "Differential thermal analysis (DTA) at high pressures: phase behavior of pure and gas-saturated liquid crystals up to 270Mpa", *Thermochim. Acta* **231**, 169-175, 1994.

24. I. Haller, "Thermodynamic and static properties of liquid crystals", *Prog. Solid State. Chem.* **10**, 103-118, 1975.

25. R.Y. Dong and G. Ravindranath, "Correlated chain dynamics in the nematic phase of 4-cyano-4′-hexyloxycyanobiphenyl", *Liq. Cryst.* **17**, 47-63, 1994.

26. K.C. Lim and J. T. Ho, "Coupling between Orientational and Translational Order in a Liquid Crystal", *Phys. Rev. Lett* **40**, 944-947, 1978.

27. Prakash P. Karat, "Electric and Magnetic Field effects in Liquid crystals", *Ph.D. Thesis*, University of Mysore, 1977.

28. S.N. Prasad and S. Venugopalan, " Molecular flexibility and orientational statistics of liquid crystals: Raman study of 7-CB and 8-OCB", *J. Chem. Phys.* **75**, 3033-3036, 1981.